Saturation and postsaturation phenomena of Rayleigh-Taylor instability with adjacent modes

Tadashi Ikegawa and Katsunobu Nishihara
Institute of Laser Engineering, Osaka University, 2-6 Yamada-oka, Suita, Osaka 565-0871, Japan
(Received 2 June 2002; published 6 February 2003)

A weakly nonlinear theory has been developed for the classical Rayleigh-Taylor instability with a finite bandwidth taken into account self-consistently. The theory includes up to third order nonlinearity, which results in the saturation of linear growth and determines subsequent weakly nonlinear growth. Analytical results are shown to agree fairly well with two-dimensional hydrodynamic simulations. There are generally many local peaks of a perturbation with a finite bandwidth due to the interference of modes. Since a local amplitude is determined from phases among the modes as well as the bandwidth, we have investigated an onset of the linear growth saturation and the subsequent weakly nonlinear growth for different bandwidths and phases. It is shown that the saturation of the linear growth occurs locally, i.e., each of the local maximum amplitudes (LMAs) grows exponentially until it reaches almost the same saturation amplitude. In the random phase case, the root mean square amplitude thus saturates with almost the same amplitude as the LMA, after most of the LMAs have saturated. The saturation amplitude of the LMA is found to be independent of the bandwidth and depends on the Atwood number. We derive a formula of the saturation amplitude of modes based on the results obtained, and discuss its relation with Haan's formula [Phys. Rev. A **39**, 5812 (1989)]. The LMAs grow linearly in time after the saturation and their speeds are approximated by the product of the linear growth rate and the saturation amplitude. We investigate the Atwood number dependence of both the saturation amplitude and the weakly nonlinear growth.

DOI: 10.1103/PhysRevE.67.026404 PACS number(s): 52.57.Fg, 47.20.Ma

I. INTRODUCTION

An interface between two fluids with different mass densities is unstable when the interface is accelerated into the heavy fluid. This instability is known as Rayleigh-Taylor instability (RTI) [1]. Recently the RTI has found a wider spectrum of interest in such fields as geophysics and astrophysics as well as inertial fusion energy (IFE). The RTI in IFE target implosion occurs both at an ablation surface in the acceleration phase and at an interface between a hot core and a cold main fuel in the stagnation phase. The RTI is one of critical issues in IFE, because excessive distortion of the interfaces could lead to severe degradation of implosion performance and thus less fusion output energy. The RTI grows exponentially in the linear regime [1]. The knowledge of the linear growth is, however, not enough for target design in IFE. It is of great importance to understand weakly nonlinear phenomena such as saturation of the linear growth and weakly nonlinear growth, since the achievement of ignition or high gain in IFE requires the growth of the RTI to remain linear or weakly nonlinear.

In the linear regime, we can expand a perturbation into Fourier modes and analyze the modes individually, since the modes grow independently. However, as Haan pointed out [2], in order to evaluate the saturation of the linear growth, we must take a net perturbation into account by summing adjacent modes. Namely we have to consider perturbations with a finite spectral width. He derived a well-known formula of the saturation amplitude $S(k)$:

$$\text{for three dimensions,} \quad S(k)=\frac{\nu}{Lk^2}, \quad \nu=2-4, \qquad (1)$$

where $k(=2\pi/\lambda)$ is a wave number and L is the system size. The formula has been, however, derived from phenomenological assumptions that the saturation of the linear growth occurs as the root mean square (rms) of the amplitude reaches $\eta\lambda(\eta\sim 0.1)$, and the parameters ν and η are not derived self-consistently, but determined from experiments or simulations [3,4]. Subsequently, other workers [5–7] extended the model with an second-order mode coupling theory [8]. But all of them stand on the same assumptions.

In addition to the finite spectral width of the perturbation, we have to consider up to third-order nonlinearity in order to evaluate the saturation and the weakly nonlinear growth self-consistently. As mentioned by Jacobs and Catton [9], a self-modulation of a primary mode produced by the third-order nonlinearity is a mechanism for deviation from the linear growth. However they considered only a single mode and the Atwood number 1, i.e., they neglected the light fluid.

Hence based on the superposition of modes, we have developed third-order nonlinear theories that describe continuous transition from the linear to the weakly nonlinear growths of the classical RTI [10,11] and the ablative RTI [12]. The theories considered an arbitrary perturbation with a small but finite bandwidth self-consistently. In this paper we develop the model for the classical RTI and present, in detail, the derivation of coupled partial differential equations that determine the onset of the saturation and the subsequent weakly nonlinear growth.

As will be shown in this paper, the saturation of the linear growth and the weakly nonlinear growth are determined from the local structure of a perturbation with a finite bandwidth. Local amplitudes of the perturbation are determined from both a spectral distribution of the modes and phase differences among the modes. For the perturbation with the finite bandwidth, we have to distinguish a local maximum amplitude (LMA), the rms amplitude, and the am-

plitude of the k mode. Here we investigate linear and weakly nonlinear evolution of these amplitudes for different bandwidths and different phase relations among the modes. We consider two extreme cases of the phase, random phase (RP) and no phase difference (NPD) among the modes. In the RP case, there are many local peaks of the perturbation amplitudes comparable to each other as a result of interference among the modes. In the NPD case, there is only one local peak with a large amplitude. By comparing these two cases of the phase relation, our results reveal that the saturation of the linear growth occurs locally, which seems to contradict the basic assumption of Eq. (1) that the rms amplitude determines the saturation.

Our results also indicate that since the LMAs saturate at almost the same amplitudes, the saturation amplitude of the rms coincides with those of the LMAs for a case with a large number of states. Bearing this fact in mind, we derive a new criterion of the saturation amplitude based on the results obtained, and discuss its physical difference from Eq. (1). Understanding the relationship between nonlinear phenomena and the Atwood number is very important for IFE, and is also interesting from a physical point of view. On an asymptotic formula of the bubble velocity in the fully nonlinear regime, the Atwood number dependence of the velocity has previously been reported [13–15]. The asymptotic formula was derived from a drag-buoyancy model [13,14] or the Layzer-type model [15,16]. In this paper, we show the Atwood number dependence of both the saturation amplitude and the nonlinear growth rate in the weakly nonlinear regime.

In Sec. II, we derive the coupled partial differential equations. Section III consists of four subsections. In Sec. III A, we show that analytical results agree fairly well with two-dimensional hydrodynamic simulations. In Sec. III B, by carrying out a three-dimensional analysis of a two-dimensional flow, we investigate the nonlinear evolution of the LMAs, the rms amplitude and the amplitude of the k_0 mode for different bandwidths and phases, and show that the linear growth saturation is determined essentially from the LMA instead of the rms amplitude. We discuss the Atwood number dependence of the saturation amplitude and the weakly nonlinear growth in Sec. III C and derive a formula for the saturation amplitude and discuss its relation with Haan's formula, Eq. (1), in Sec. III D. We summarize our work in Sec. IV.

II. MATHEMATICAL FORMULATION

We consider a x-y planar interface $[z=\xi(\boldsymbol{x},t)]$ between a heavy fluid $(z>\xi)$ with density ρ_H and a light fluid $(z<\xi)$ with density $\rho_L(\rho_H>\rho_L)$, where $\boldsymbol{x}$ is a two-dimensional vector, subscripts H and L denote the heavy fluid and the light fluid, respectively. Let Ω be an area of the interface. We assume periodic boundary conditions in the x and y directions with a size L,

$$\Omega=\{(x,y):\ 0\leqslant x\leqslant L,\ \ 0\leqslant y\leqslant L\}.$$

We set a uniform gravitational acceleration g along the $-z$ direction. The acceleration induces the growth of the interface perturbation.

We set up the problem in a standard way, the normal mode approach [9,17,18]. We assume that the fluids are inviscid, incompressible, and irrotational. Then, we write the fluid velocity using velocity potentials such as

$$\begin{aligned}\boldsymbol{u}' &= -\boldsymbol{\nabla}'\phi_H \quad (\text{for } z>\xi)\\ &= -\boldsymbol{\nabla}'\phi_L \quad (\text{for } z<\xi),\end{aligned}$$

where the vectors with the primes are three dimensional and the vectors without it are two dimensional. The potentials satisfy the Laplace equation

$$\nabla'^2\phi=0. \tag{2}$$

We require that ϕ_H and ϕ_L go to zero as z goes to $+\infty$ and $-\infty$, respectively.

Pressure is given by Bernoulli's equation

$$p=\rho\left[\frac{\partial\phi}{\partial t}-\frac{1}{2}(\boldsymbol{\nabla}'\phi)^2-g\xi\right]. \tag{3}$$

From the pressure continuity at the interface, $p_H|_\xi=p_L|_\xi$, we obtain

$$\begin{aligned}&\rho_H\left[\left.\frac{\partial\phi_H}{\partial t}\right|_\xi-\frac{1}{2}\left.(\boldsymbol{\nabla}'\phi_H)^2\right|_\xi-g\xi\right]\\ &\quad=\rho_L\left[\left.\frac{\partial\phi_L}{\partial t}\right|_\xi-\frac{1}{2}\left.(\boldsymbol{\nabla}'\phi_L)^2\right|_\xi-g\xi\right].\end{aligned} \tag{4}$$

Since the interface moves with the fluids, $d\xi/dt=\partial\xi/\partial t+(\boldsymbol{u}\cdot\boldsymbol{\nabla})\xi=-\partial\phi/\partial z|_\xi=u_z|_\xi$, which gives,

$$\frac{\partial\xi}{\partial t}=(\boldsymbol{\nabla}\phi|_\xi)\cdot\boldsymbol{\nabla}\xi-\left.\frac{\partial\phi}{\partial z}\right|_\xi. \tag{5}$$

Since ϕ is either ϕ_H or ϕ_L, this equation is actually two equations. In Eqs. (4) and (5), the partial derivative of the velocity potential at the interface can be calculated with the Taylor series expansion with respect to the perturbation amplitude under the assumption of $k|\xi|\sim O(\epsilon)<1$. For example, Eq. (5) becomes

$$\begin{aligned}\frac{\partial\xi}{\partial t}=&\left[\boldsymbol{\nabla}\phi|_{z=0}+\xi\left.\frac{\partial}{\partial z}(\boldsymbol{\nabla}\phi)\right|_{z=0}\right]\cdot\boldsymbol{\nabla}\xi\\ &-\left.\frac{\partial\phi}{\partial z}\right|_{z=0}-\xi\left.\frac{\partial^2\phi}{\partial z^2}\right|_{z=0}-\left.\frac{\xi^2}{2}\frac{\partial^3\phi}{\partial z^3}\right|_{z=0}+\text{h. o. t.},\end{aligned} \tag{6}$$

where h. o. t. represents terms higher than the third order.

In order to treat the interface perturbation with a finite bandwidth $\boldsymbol{k}=\boldsymbol{k}_0+\delta\boldsymbol{k}$, where $\boldsymbol{k}$ has discrete allowed values $(2\pi l/L,2\pi m/L)$ for integers l and m and $|\boldsymbol{k}_0|>|\delta\boldsymbol{k}|$, we take the following description for the amplitude of the perturbation:

$$\xi(\boldsymbol{x},t)=\sum_{\delta\boldsymbol{k}}\ \xi_{\boldsymbol{k}}(t)c\cos[(\boldsymbol{k}_0+\delta\boldsymbol{k})\cdot\boldsymbol{x}]$$
$$=\left\{\left[\sum_{\delta\boldsymbol{k}}\ \xi_{\boldsymbol{k}}(t)\cos(\delta\boldsymbol{k}\cdot\boldsymbol{x})\right]c\cos(\boldsymbol{k}_0\cdot\boldsymbol{x})-\left[\sum_{\delta\boldsymbol{k}}\ \xi_{\boldsymbol{k}}(t)\sin(\delta\boldsymbol{k}\cdot\boldsymbol{x})\right]c\sin(\boldsymbol{k}_0\cdot\boldsymbol{x})\right\}$$
$$\equiv\frac{c}{2}\overline{\xi}(\boldsymbol{x},t)e^{i\boldsymbol{k}_0\cdot\boldsymbol{x}}+\text{c.c.},\tag{7}$$

where c is a normalizing constant determined later, $\overline{\xi}$ represents a complex amplitude, and c.c. denotes the complex conjugate. Equation (7) allows the perturbation amplitude to vary slowly in space compared with the wavelength corresponding to $\lambda_0=2\pi/k_0$. We assume that the spatial derivative of the amplitude is second order with respect to the amplitude. Namely, in

$$\boldsymbol{\nabla}\xi=\frac{c}{2}e^{i\boldsymbol{k}_0\cdot\boldsymbol{x}}(i\boldsymbol{k}_0+\boldsymbol{\nabla})\overline{\xi}+\text{c.c.},\tag{8}$$

$\boldsymbol{\nabla}\overline{\xi}\sim\delta\boldsymbol{k}\overline{\xi}\sim(\delta\boldsymbol{k}/k_0)(\overline{\xi}/\lambda)\sim O(\epsilon^2)$ and $k_0=|\boldsymbol{k}_0|$.

The velocity potentials as well as the interface displacement are then composed of the slowly varying amplitudes as

$$\phi_H(\boldsymbol{x}',t)=\frac{c}{2}\overline{\phi}_H(\boldsymbol{x}',t)e^{i\boldsymbol{k}_0\cdot\boldsymbol{x}-k_0z}+\text{c.c.},\tag{9a}$$

$$\phi_L(\boldsymbol{x}',t)=\frac{c}{2}\overline{\phi}_L(\boldsymbol{x}',t)e^{i\boldsymbol{k}_0\cdot\boldsymbol{x}+k_0z}+\text{c.c.},\tag{9b}$$

so that the first order of the Laplace equation with respect to the amplitude is satisfied. The higher order of the Laplace equation (2) gives relations for the amplitudes of the velocity potential:

$$k_0\frac{\partial\overline{\phi}_{H,L}}{\partial z}=\pm i\boldsymbol{k}_0\cdot\boldsymbol{\nabla}\overline{\phi}_{H,L}\pm\frac{1}{2k_0^2}|\boldsymbol{k}_0\times\boldsymbol{\nabla}|^2\overline{\phi}_{H,L}+\text{h. o. t.},\tag{10}$$

where the upper and lower signs are for $\overline{\phi}_H$ and $\overline{\phi}_L$, respectively. The left hand side of Eq. (10) and the first term of the right hand side are second order, while the second term is third order.

Nonlinear terms generate higher harmonics. Therefore, we rewrite ξ, ϕ_H, and ϕ_L as

$$\xi(\boldsymbol{x},t)=\sum_n\ \frac{c_n}{2}\overline{\xi}^{(n)}(\boldsymbol{x},t)e^{in\boldsymbol{k}_0\cdot\boldsymbol{x}}+\text{c.c.},\tag{11a}$$

$$\phi_H(\boldsymbol{x}',t)=\sum_n\ \frac{c_n}{2}\overline{\phi}_H^{(n)}(\boldsymbol{x}',t)e^{in\boldsymbol{k}_0\cdot\boldsymbol{x}-nk_0z}+\text{c.c.},\tag{11b}$$

$$\phi_L(\boldsymbol{x}',t)=\sum_n\ \frac{c_n}{2}\overline{\phi}_L^{(n)}(\boldsymbol{x}',t)e^{in\boldsymbol{k}_0\cdot\boldsymbol{x}+nk_0z}+\text{c.c.}\tag{11c}$$

The normalizing constants are then given by

$$c_n=\sqrt{\frac{2}{1+\delta_{0n}}},\tag{12}$$

where δ_{mn} is the Kronecker delta. We assume that the fundamental mode ($n=1$) is in first order. The $n=2$ and $n=0$ modes arise from the mode coupling of the fundamental modes ($k_0+k_0=2k_0$, $k_0-k_0=0$), and they are in second order of ϵ^2. We consider up to the third-order nonlinearity to describe the self-modulation of the fundamental mode. Hereafter, we introduce dimensionless variables k_0x, γ_1t, $k_0\xi$, $k_0^2\phi/\gamma_1$, and γ_2/γ_1, where $\gamma_1\equiv\sqrt{\alpha k_0g}$ and $\gamma_2\equiv\sqrt{2}\gamma_1$ are the linear growth rates of the k_0 and $2k_0$ modes, respectively. Substituting Eqs. (11) into Eqs. (4) and (5) and picking up terms associated with $\exp(in\boldsymbol{k}_0\cdot\boldsymbol{x})$ ($n=1,2,0$), we obtain the following system of equations from Eq. (4):

$$\frac{1+\alpha}{2}\left[\frac{\partial\phi_H^{(1)}}{\partial t}-\sqrt{2}\xi^{(1)*}\frac{\partial\phi_H^{(2)}}{\partial t}-\frac{\sqrt{2}}{2}\frac{\partial\phi_H^{(1)*}}{\partial t}\xi^{(2)}-\xi^{(0)}\frac{\partial\phi_H^{(1)}}{\partial t}-2\sqrt{2}\phi_H^{(1)*}\phi_H^{(2)}+2\xi^{(1)}|\phi_H^{(1)}|^2+\frac{1}{4}\left(2|\xi^{(1)}|^2\frac{\partial\phi_H^{(1)}}{\partial t}+\frac{\partial\phi_H^{(1)*}}{\partial t}\xi^{(1)2}\right)-\frac{\xi^{(1)}}{\alpha}\right]=\frac{1-\alpha}{2}\left[\frac{\partial\phi_L^{(1)}}{\partial t}+\sqrt{2}\xi^{(1)*}\frac{\partial\phi_L^{(2)}}{\partial t}+\frac{\sqrt{2}}{2}\frac{\partial\phi_L^{(1)*}}{\partial t}\xi^{(2)}+\xi^{(0)}\frac{\partial\phi_L^{(1)}}{\partial t}-2\sqrt{2}\phi_L^{(1)*}\phi_L^{(2)}-2\xi^{(1)}|\phi_L^{(1)}|^2+\frac{1}{4}\left(2|\xi^{(1)}|^2\frac{\partial\phi_L^{(1)}}{\partial t}+\frac{\partial\phi_L^{(1)*}}{\partial t}\cdot\xi^{(1)2}\right)-\frac{\xi^{(1)}}{\alpha}\right],\tag{13a}$$

$$\frac{1+\alpha}{2}\left(\frac{\partial\phi_H^{(2)}}{\partial t}-\frac{\sqrt{2}}{2}\xi^{(1)}\frac{\partial\phi_H^{(1)}}{\partial t}-\frac{\xi^{(2)}}{\alpha}\right)=\frac{1-\alpha}{2}\left(\frac{\partial\phi_L^{(2)}}{\partial t}+\frac{\sqrt{2}}{2}\xi^{(1)}\frac{\partial\phi_L^{(1)}}{\partial t}-\frac{\xi^{(2)}}{\alpha}\right),\tag{13b}$$

$$\frac{1+\alpha}{2}\left[\frac{\partial\phi_H^{(0)}}{\partial t}-\frac{1}{4}\left(\xi^{(1)*}\frac{\partial\phi_H^{(1)}}{\partial t}+\frac{\partial\phi_H^{(1)*}}{\partial t}\xi^{(1)}\right)-\frac{1}{2}|\phi_H^{(1)}|^2-\frac{\xi^{(0)}}{\alpha}\right]=\frac{1-\alpha}{2}\left[\frac{\partial\phi_L^{(0)}}{\partial t}+\frac{1}{4}\left(\xi^{(1)*}\frac{\partial\phi_L^{(1)}}{\partial t}+\frac{\partial\phi_L^{(1)*}}{\partial t}\xi^{(1)}\right)-\frac{1}{2}|\phi_L^{(1)}|^2-\frac{\xi^{(0)}}{\alpha}\right],\tag{13c}$$

where the asterisk represents the complex conjugate, $\alpha \equiv (\rho_H - \rho_L)/(\rho_H + \rho_L)$ is the Atwood number, $\hat{\boldsymbol{k}}_0 \equiv \boldsymbol{k}_0 / k_0$, and we omit the bar. We also obtain from Eq. (5),

$$\frac{\partial \xi^{(1)}}{\partial t} = \phi_H^{(1)} - i(\hat{\boldsymbol{k}}_0 \cdot \boldsymbol{\nabla})\phi_H^{(1)} - \frac{1}{2}|\hat{\boldsymbol{k}}_0 \times \boldsymbol{\nabla}|^2 \phi_H^{(1)} - \xi^{(0)} \phi_H^{(1)} + \frac{\sqrt{2}}{2}\phi_H^{(1)*}\xi^{(2)} - \sqrt{2}\xi^{(1)*}\phi_H^{(2)} + \frac{1}{4}(2|\xi^{(1)}|^2 \phi_H^{(1)} - \phi_H^{(1)*}\xi^{(1)2}), \tag{14a}$$

$$= -\phi_L^{(1)} + i(\hat{\boldsymbol{k}}_0 \cdot \boldsymbol{\nabla})\phi_L^{(1)} + \frac{1}{2}|\hat{\boldsymbol{k}}_0 \times \boldsymbol{\nabla}|^2 \phi_L^{(1)} - \xi^{(0)} \phi_L^{(1)} + \frac{\sqrt{2}}{2}\phi_L^{(1)*}\xi^{(2)} - \sqrt{2}\xi^{(1)*}\phi_L^{(2)} - \frac{1}{4}(2|\xi^{(1)}|^2 \phi_L^{(1)} - \phi_L^{(1)*}\xi^{(1)2}), \tag{14b}$$

$$\frac{\partial \xi^{(2)}}{\partial t} = 2\phi_H^{(2)} - \sqrt{2}\xi^{(1)}\phi_H^{(1)} \tag{14c}$$

$$= -2\phi_L^{(2)} - \sqrt{2}\xi^{(1)}\phi_L^{(1)}. \tag{14d}$$

Note that an equation for $n=0$ is $\partial \xi^{(0)}/\partial t = 0$ within second order.

We can derive the coupled partial differential equations for the velocity potentials $\phi_H^{(1)}$ and $\phi_H^{(2)}$, by eliminating the other terms such as $\phi_L^{(1)}$, $\phi_L^{(2)}$, $\xi^{(1)}$, $\xi^{(2)}$ in Eqs. (13a)–(13c) and (14a)–(14d). Details of the derivation are shown in Appendix A. We then obtain

$$\frac{\partial^2 \phi_H^{(1)}}{\partial t^2} = \phi_H^{(1)} - i(\hat{\boldsymbol{k}}_0 \cdot \boldsymbol{\nabla})\phi_H^{(1)} - \frac{1}{2}|\hat{\boldsymbol{k}}_0 \times \boldsymbol{\nabla}|^2 \phi_H^{(1)} + \frac{(4+\gamma_2^2)\alpha + (4-\gamma_2^2)}{\sqrt{2}}\phi_H^{(1)*}\frac{\partial \phi_H^{(2)}}{\partial t} + \frac{\alpha(2+3\gamma_2^2)}{\sqrt{2}}\frac{\partial \phi_H^{(1)*}}{\partial t}\phi_H^{(2)}$$
$$+ 2(1-3\alpha)\left|\frac{\partial \phi_H^{(1)}}{\partial t}\right|^2 \phi_H^{(1)} - (3\alpha+1)\phi_H^{(1)*}\left(\frac{\partial \phi_H^{(1)}}{\partial t}\right)^2 + \alpha(\alpha-3)|\phi_H^{(1)}|^2 \phi_H^{(1)}, \tag{15a}$$

$$\frac{\partial^2 \phi_H^{(2)}}{\partial t^2} = \gamma_2^2 \phi_H^{(2)} + \sqrt{2}(1-\alpha)\phi_H^{(1)}\frac{\partial \phi_H^{(1)}}{\partial t}. \tag{15b}$$

Equations (15a) and (15b) are the coupled partial differential equations that describe the transition from the linear to the weakly nonlinear regimes continuously.

We here discuss the linear growth rate of each mode. As is well known, shorter wavelength modes grow faster than longer wavelength modes. The linear terms of Eq. (15a) represent this property accurately up to second order $(\delta k)^2$. To clarify this feature, by treating the slowly varying amplitude as $\exp(i\delta \boldsymbol{k} \cdot \boldsymbol{x})$, we rewrite the first to third terms in Eq. (15a) with dimensional variables as

$$\gamma_1^2 \phi_H^{(1)} - i\frac{\gamma_1^2}{k_0}(\hat{\boldsymbol{k}}_0 \cdot \boldsymbol{\nabla})\phi_H^{(1)} - \frac{\gamma_1^2}{2k_0^2}|\hat{\boldsymbol{k}}_0 \times \boldsymbol{\nabla}|^2 \phi_H^{(1)}$$
$$= \alpha g\left[k_0 + \hat{\boldsymbol{k}}_0 \cdot \delta \boldsymbol{k} + \frac{1}{2k_0^3}(\delta k_x^2 k_y^2 - 2\delta k_x \delta k_y k_x k_y + \delta k_y^2 k_x^2)\right] e^{i\delta \boldsymbol{k} \cdot \boldsymbol{x}} \approx \alpha |\boldsymbol{k}_0 + \delta \boldsymbol{k}| g \phi_H^{(1)}. \tag{16}$$

This is the second-order approximation in the Taylor series of the square of the linear growth rate $\sqrt{\alpha |\boldsymbol{k}_0 + \delta \boldsymbol{k}| g}$. The third term on the left hand side represents a three-dimensional effect in the Fourier space, and it vanishes in a two-dimensional case.

Third-order nonlinear terms on the left hand side of Eq. (15a) consist of mode coupling between the fundamental and the second harmonics [for example, $2(k_0 + \delta k_1) - (k_0 + \delta k_2) = k_0 + (2\delta k_1 - \delta k_2)$], and the self-modulation of the fundamental harmonic $[(k_0 + \delta k_1) + (k_0 + \delta k_2) - (k_0 + \delta k_3) = k_0 + (\delta k_1 + \delta k_2 - \delta k_3)]$. They determine the weakly nonlinear growth of the fundamental. In the limit of $\alpha = 1$ and a single mode (in this limit $\phi_H^{(1)*} = \phi_H^{(1)}$), the coupled equations coincide with those derived by Jacobs and Catton [9]. The partial differential equation for the third harmonic, $3\boldsymbol{k}_0$, is derived in Appendix B. Though the third harmonic determines nonlinear structures of the interface such as the bubble-spike structure, it is not as important for the evaluation of the saturation amplitude as the second harmonic is. The third harmonic does not affect the growth of the fundamental mode in the framework of this model.

III. RESULTS AND DISCUSSIONS

In this section we analyze the weakly nonlinear growth of the RTI by solving Eqs. (15a) and (15b) numerically as an initial value problem. We consider perturbations of the two-

dimensional interface with meshes of $M_x \times M_y$. The normalized system size is $k_0 L = k_0 \Delta x M_x$, where Δx is a mesh size and $m = L/\lambda_0 = k_0 \Delta x M_x / 2\pi$ should be an integer. As an initial perturbation, we consider either $\xi \neq 0$, $\dot{\xi} = 0$ or $\xi = 0$, $\dot{\xi} \neq 0$. For the former case, we set the following conditions on the time derivatives of the velocity potentials of the fundamental, because $\dot{\xi}^{(1)} = \dot{\phi}_H^{(1)}$ in the linear regime. Since $\dot{\phi}_H$ is a complex function as shown in Eq. (9), we define $\dot{\phi}_H \equiv \dot{\phi}_{H,c} + i\dot{\phi}_{H,s}$ and

$$\dot{\phi}_{H,c}^{(1)}(t=0) = \sum_{l_x, l_y} A_{l_x, l_y} \cos[i(\delta \boldsymbol{k}_{l_x, l_y} \cdot \boldsymbol{x} + \varphi_{l_x, l_y})], \tag{17a}$$

$$\dot{\phi}_{H,s}^{(1)}(t=0) = \sum_{l_x, l_y} A_{l_x, l_y} \sin[i(\delta \boldsymbol{k}_{l_x, l_y} \cdot \boldsymbol{x} + \varphi_{l_x, l_y})], \tag{17b}$$

and $\phi_H(t=0) = 0$, where φ_{l_x, l_y} is an initial phase of the mode, $\delta \boldsymbol{k}_{l_x, l_y} = (2\pi l_x / L, 2\pi l_y / L)$ is the wave vector within a finite bandwidth, and $\boldsymbol{x} = (i_x \Delta x, i_y \Delta x)$ is a position vector. i_x, i_y, l_x, and l_y are integers, where $-M_x/2 < l_x < M_x/2$, and $-M_y/2 < l_y < M_y/2$. A_{l_x, l_y} is the amplitude of the perturbation. We here consider a Gaussian distribution function or a flat top distribution function for the amplitudes of modes within the bandwidth ($|\delta \boldsymbol{k}_{l_x, l_y}| \leqslant \delta k$):

$$A_{l_x, l_y} = \begin{cases} c_g \exp\left[-\frac{1}{2} \left(\frac{|\delta \boldsymbol{k}_{l_x, l_y}|}{\delta k} \right)^2 \right] \\ c_f, \end{cases} \tag{18}$$

where c_g and c_f are normalization constants. We assume that the amplitudes of modes outside the initial bandwidth are initially zero. We analyze the modes outside the bandwidth generated by the mode coupling of the fundamentals as second harmonic. When we give an initial perturbation on the interface velocity, we set the same conditions as Eq. (17) for $\phi_H^{(1)}(t=0)$ and $\dot{\phi}_H(t=0) = 0$.

Since modes grow independently of each other in the linear regime, we can expand perturbations into Fourier modes, and analyze the modes individually. In the nonlinear regime, however, we must analyze a net amplitude of the perturbations by summing the modes. This requirement implies that the local structure of the perturbation is important in the nonlinear regime. The local amplitude is determined from both the spectral distribution and the phase difference among the modes. Here, we consider two extreme cases of the phase, RP and NPD among the modes ($\varphi_{l_x, l_y} = 0$). As discussed in Sec. I, in the RP case, there are many local peaks of the perturbation amplitudes comparable to each other as a result of interference among the modes. In the NPD case, there is only one local peak with a large amplitude. For these two cases, we compare the nonlinear growth of the LMA with that of the rms amplitude.

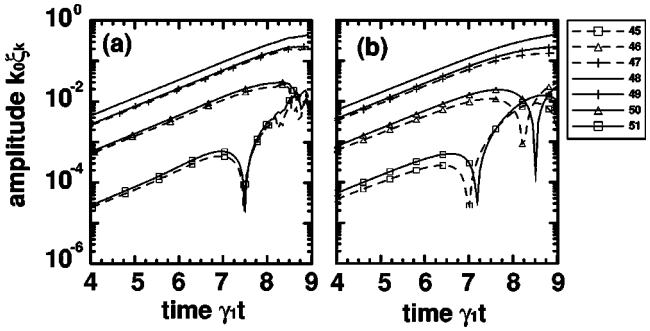

FIG. 1. Normalized Fourier amplitudes $k_0 \xi_k$ of the interface displacement as functions of normalized time $\gamma_1 t$ in NPD case. (a) Simulation results for each mode from 45 to 51 and (b) analytical results of corresponding modes. The same symbols are used for the corresponding modes.

A. Comparison with simulation

We first show the validity of the governing equations by comparing with two-dimensional hydrodynamic simulations. To solve Eqs. (15a) and (15b) numerically, we define the slowly varying velocity potential at meshes of number and mesh size $M_x = 32$ and $k_0 \Delta x = 3\pi$, respectively. The minimum wave number then becomes $\delta k_{min}/k_0 = (2\pi/L)/k_0 = 2\pi/k_0 M \Delta x = 1/48$. We carried out two-dimensional simulations with the use of an Eulerian hydrodynamic simulation code, IMPACT2D [19]. In the analytical model, we consider only the slowly varying amplitude of the velocity potential, while in the hydrodynamic simulation we must use fine meshes to resolve perturbations with a wavelength of the order of $2\pi/k_0$. We used mesh numbers of $M_x \times M_z = 2048 \times 300$ in the simulations. We chose the wavelength corresponding to k_0 as $\lambda_0 = L/m$ and $m = 48$, so that the difference of the wave number between the modes with m and $m \pm 1$ coincides with the minimum wave number δk_{min} in the analytical model. Since in the Eulerian hydrodynamic code the spatial resolution is limited by a finite size of the mesh, it is difficult to give a very small amplitude of corrugation much less than the mesh size. We thus give initial perturbations in the fluid velocity instead of the interface corrugation. The initial velocity perturbations are incompressible and irrotational and they decay as $\exp(-k|z|)$. The initial velocity perturbations are given for mode numbers within $m \pm M/2 = 48 \pm 16$. We choose the Gaussian distribution function with the bandwidth of $\delta k/k_0 = 10^{-2}$ as an initial spectrum of the velocity perturbation, whose root mean square equals to $k_0 \dot{\xi}_{rms}/\gamma_1 \equiv \langle (k_0 \dot{\xi}/\gamma_1)^2 \rangle^{1/2} = 10^{-3}$, and $\xi(t=0) = 0$. Parameters used in the simulation are $p = 1$ Gbar, $\alpha = 0.82$ ($\rho_L = 0.5$ g/cm^3, $\rho_H = 5$ g/cm^3), $g = 10^{15}$ cm/s^2 and L ($= M_x \Delta x$) $= 1024$ μm. We assumed very high pressure to simulate incompressible fluids.

Figure 1 shows the normalized Fourier amplitudes of the surface displacement for modes from 45 to 51 as functions of normalized time in the NPD case. Figures 1(a) and 1(b) presents simulation results and solutions of Eqs. (15a) and (15b), respectively. The saturation of the linear growth starts to occur around time $\gamma_1 t = 7-8$. Dips of the perturbations shown in Fig. 1 correspond to phase change due to the non-

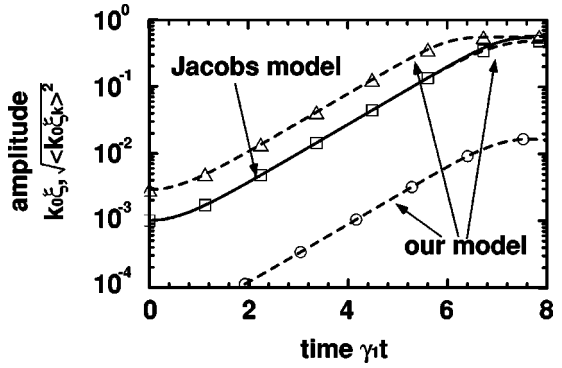

FIG. 2. Temporal evolution of the amplitudes in the random phase case: Solid line is the amplitude of Jacobs's single-mode model, dashed lines are, respectively, the amplitudes of the rms (squares), $k_0\xi_{k_0}$ (circles), and the maximum value among the LMAs (triangles) of our model.

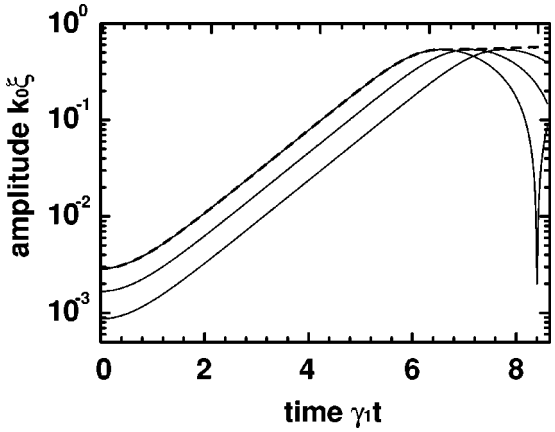

FIG. 3. Temporal evolution of the normalized local maximum amplitudes $k_0\xi$ at three different fixed points with different initial amplitudes. The dashed line is the temporal growth of the local peak moving in the x-y plane in nonlinear regime.

linear mode interaction. As shown in Fig. 1, the solutions of Eqs. (15a) and (15b) agree fairly well with the simulation results including the phase changes of the individual mode.

B. Saturation of linear growth

The analysis of the weakly nonlinear phenomena of RTI should include a finite bandwidth. In the finite bandwidth case, there are different amplitudes, such as the LMA, the rms amplitude, and the amplitude of the k_0 mode. Their time evolution may not be the same in the weakly nonlinear regime. We show their time evolution in the present model with a finite bandwidth of $\delta k/k_0=1\times10^{-2}$, comparing with the result of a single mode model [9]. The analysis is performed in the three-dimensional RP case with the parameters $(M_x,M_y,k_0\Delta x,\alpha)=(512,512,3\pi,1)$ and the flat top distribution function of the initial spectrum. Here we used $\alpha=1$, since in Ref. [9] they considered only such a case. We chose $k_0\xi_{rms}=10^{-3}$ and $\dot{\xi}=0$ as the initial conditions. The initial amplitude of the single mode was chosen to equal to that of the rms in the finite bandwidth case.

In Fig. 2, the solid line represents the temporal evolution of the amplitude with the single mode, while dashed lines represent those with the finite bandwidth: the maximum value of the LMAs (triangles), the rms amplitude (squares), and the amplitude of the k_0 mode, i.e., $k_0\xi_{k_0}$ (circles). As is clearly seen in the figure, the amplitudes of the single mode, the LMA, the rms, and the k_0 mode initially grow exponentially with almost the same linear growth rate for the small bandwidth of $\delta k/k_0=1\times10^{-2}$ [see Eq. (16)]. It seems that results of both the single mode and the finite bandwidth successfully reproduce the saturation of the linear growth. The maximum value of the LMAs starts to saturate at first when it reaches $k_0\xi\sim0.23$ in the finite bandwidth case. At that time the rms amplitude keeps growing until it reaches almost the same saturation amplitude of the maximum value of the LMAs. This can be explained as follows.

In the RP case, there are many local peaks due to the interference among the modes. For $\delta k/k_0=1\times10^{-2}$, the number of the local peaks is $\approx3\times10^2$. If we choose three different fixed points where the initial amplitude of the interface corrugation has different local maximum values, the amplitudes at these points grow in time as shown in Fig. 3. All of them initially grow exponentially, and each of them starts to saturate at different times as it reaches the same saturation amplitude of the maximum of the LMAs. Dips of the LMA indicate that the position of the LMA moves in the weakly nonlinear regime. Although the position of the LMA moves, its value keeps growing linearly in time after the saturation as shown with the dashed line in Fig. 3. The mode coupling in the nonlinear regime results in the phase change among the modes and thus the motion of the points where the LMA exists. This result indicates that the local structure of the interface determines the saturation of the linear growth. When most of the LMAs reach the saturation amplitude, the rms amplitude also saturates at almost the same saturation amplitude as that of the LMA. The spectrum broadenings are also observed in the nonlinear regime [10,11].

As shown in Fig. 2, the amplitude of the k_0 mode also saturates at the same time as the rms amplitude. It should be also noted that the saturation amplitude of the single mode is almost the same as that of the maximum of the LMAs with finite bandwidth. However, for the case of the finite bandwidth, the saturation amplitude of the k_0 mode is much less than that of the single-mode, as expected. As the initial spectral width is wider, the saturation amplitude of the individual mode becomes much smaller than that of the rms. Hence, the single mode analysis results in an overestimate of the growth, and is not adequate for the evaluation of perturbations with the finite bandwidth.

As discussed above, the LMAs saturate at almost the same amplitude. The local amplitude is determined from the phase among the modes in addition to the spectral width. We now discuss different dependences of the rms saturation amplitude on the spectral width between the RP and NPD cases. We calculate the temporal growth of the RTI for three different initial spectral widths of $\delta k/k_0=2\times10^{-3}$, 1.6×10^{-2}, and 0.128. We use the Gaussian distribution function of the

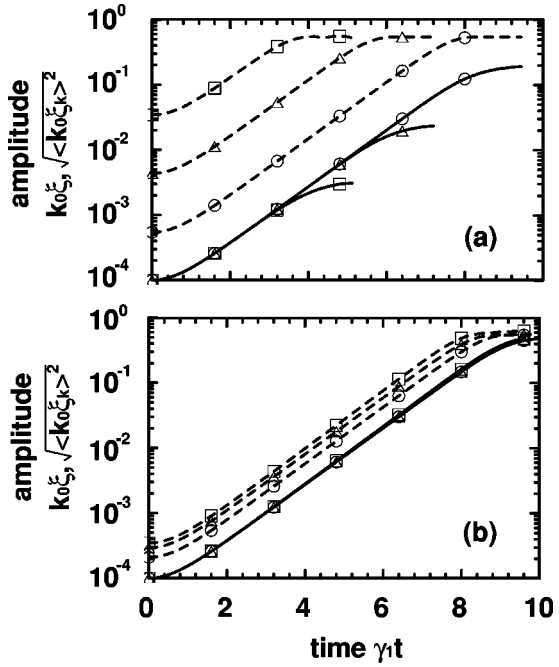

FIG. 4. Temporal evolution of the normalized local maximum amplitudes $k_0\xi$ (dashed lines) and the normalized rms amplitudes $\sqrt{\langle (k_0\xi_k)^2 \rangle}$ (solid line) for three different initial spectral widths; $\delta k/k_0 = 2\times 10^{-3}$ (squares), 1.6×10^{-2} (triangles), and 0.128 (circles). (a) NPD case and (b) RP case.

initial spectrum, and choose $\alpha = 0.8$. The parameters $(M_x, M_y, k_0\Delta x)$ are the same as before. Figure 4 shows the resultant growth of the rms amplitudes (solid line) and the maximum among the LMAs (dashed line) for the NPD [Fig. 4(a)] and the RP [Fig. 4 (b)], respectively. Since we choose the initial rms amplitudes as the same value of $\sqrt{\langle (k_0\xi)^2 \rangle} = 10^{-4}$ for three different initial bandwidths, the initial LMAs are proportional to the bandwidth as shown in Fig. 4(a). As expected, the initial LMA of the NPD is larger than that of the RP for each corresponding bandwidth. The LMAs start to saturate when they reach the same amplitude of $k_0\xi \approx 0.27$ even for the three different initial spectral widths, and for two different initial phases among the modes, i.e., the NPD and RP. It indicates that the saturation of the linear growth is determined by the LMA instead of the rms amplitude, and the saturation amplitude of the LMA is independent of the initial bandwidth.

The rms amplitude saturates when the LMA does in the NPD case, and the saturation amplitude of the rms decreases with the increase of the bandwidth as shown in Fig. 4(a). This decrease of the rms saturation amplitude is easily understood from the consideration of spatial distributions of the LMA. In the NPD case, there is only one local peak with a large amplitude. Hence, the rms amplitudes saturate with different values for the different initial spectral widths when the corresponding LMAs reach the saturation amplitude, which satisfactorily explains the results shown in Fig. 4(a). On the other hand, in the RP case the rms amplitudes keep growing after the LMAs start to saturate until they reach almost the same saturation amplitudes of the LMAs as has been shown

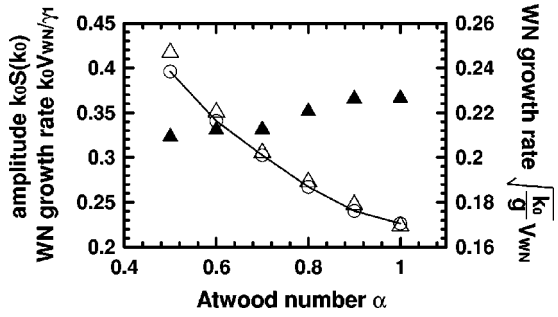

FIG. 5. Atwood number dependence of both the saturation amplitude (solid line with circles) and the weakly nonlinear growth rate (triangles) of the LMA.

before. The rms amplitudes at the transition from the linear to the weakly nonlinear growth do not depend much on the initial bandwidth in the RP case.

C. Atwood number dependence and weakly nonlinear growth

So far, we have discussed the nonlinear saturation with the fixed Atwood number. In this section, we will investigate the dependence of the saturation amplitude on the Atwood number.

As shown in Fig. 4, the saturation amplitude is determined from the LMA, which is independent of the finite initial bandwidth. As shown in Fig. 2, the saturation amplitude of the LMA with a finite bandwidth is the same as that with a single mode. Thus, the saturation amplitude of the LMA does not depend on the number of modes composing the perturbation. Therefore, the Atwood number dependence of the saturation amplitude of the LMA obtained from a single-mode analysis could be the same as that with a finite bandwidth.

We observe the saturation amplitude of the single mode by changing the Atwood number. Solid line in Fig. 5 presents its results. We here define the saturation when the growth rate decreases to 95% of the linear growth rate. As the Atwood number increases, the saturation amplitude decreases. We can explain this decrease of the saturation amplitude from the third-order nonlinearity. Specifically, the third-order nonlinearity consists of two different terms as seen in Eq. (15a). One causes the enhancement of the growth due to the mode coupling terms between the second harmonic and the fundamental. The other introduces suppression of the growth, which comes from the third-order self-modulations (last three terms). As seen in the second term of the right hand side of Eq. (15b), as the Atwood number increases, the source terms of the second harmonic become small. Thus the enhancement effects becomes small compared with the suppression effects as the Atwood number increase. This leads to the decrease of the saturation amplitude with the increase of the Atwood number.

By using an asymptotic formula of the bubble velocity in the fully nonlinear regime, some workers estimated the Atwood number dependence of the amplitude at which the asymptotic growth begins [13–15]. The saturation amplitude in the weakly nonlinear regime in Fig. 5 agrees with that

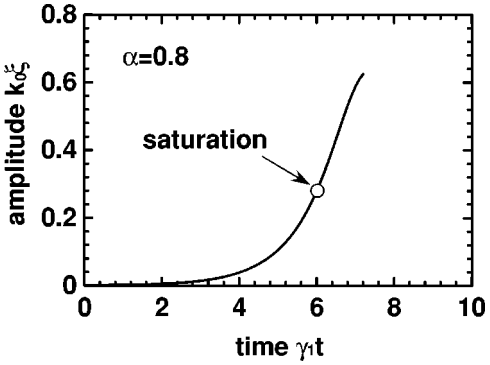

FIG. 6. Temporal growth of the local maximum amplitude.

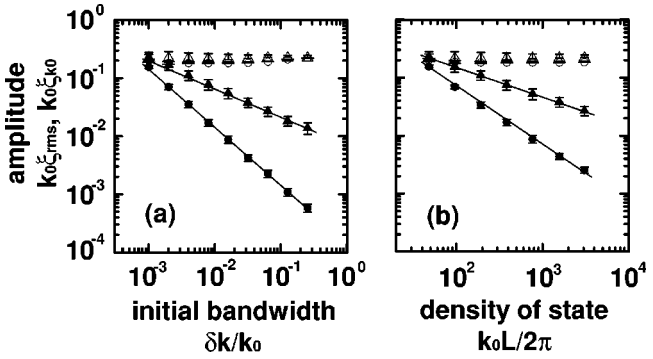

FIG. 7. Dependence of the normalized saturation amplitude of both the rms (open symbols) and the k_0 mode (closed ones) on the number of states in the RP case. (a) is a function of an initial bandwidth and (b) is a function of density of state. Here triangles and circles represent results of 2D and 3D, respectively.

estimated using the asymptotic formula at the point at which saturation amplitude is a decreasing function of the Atwood number, but does not quantitatively coincide with it.

After the saturation of the exponential growth, the RTI grows approximately with a constant speed that we call a weakly nonlinear growth rate. Figure 6 shows the temporal growth of the LMA with $\alpha=0.8$, where the saturation amplitude is $k_0\xi\approx 0.27$. As shown in the figure, our model reproduces the fact that the RTI grows with a constant speed after the linear growth saturation. Open triangles in Fig. 5 represent the weakly nonlinear growth rates obtained from the constant speeds for the different Atwood numbers. Many experiments and simulations [2,21,23,24] show that the weakly nonlinear growth rate is approximately given as

$$v_{wn}(k_0)\approx \gamma_1 S(k_0). \tag{19}$$

The growth rate of the right hand side of Eq. (19) corresponds to the circles in Fig. 5, because it is normalized as $(k_0/\gamma_1)v_{wn}(k_0)=(k_0/\gamma_1)\gamma_1 S(k_0)=k_0 S(k_0)$. The growth rates (open triangles) agree fairly well with that evaluated from Eq. (19) (circles). Closed triangles in Fig. 5 are also the weakly nonlinear growth rates renormalized by $\sqrt{k/g}$ to show their dependence on the Atwood number. Their positive gradient indicates that the weakly nonlinear growth rate increase slightly as the Atwood number increases.

D. Criterion of saturation amplitude

As we have shown in Sec. III B, the saturation of the linear growth is determined from the local maximum amplitude instead of the root mean square amplitude. The rms amplitude saturates as most of the LMAs saturate. Therefore if we can observe the LMA directly, the knowledge of the rms amplitude or the amplitudes of modes may not be important for the investigation of the linear growth saturation. The amplitude of the k_0 mode also saturates when the rms does because it is proportional to the rms amplitude. Historically, however, there are many theoretical [5–7,20–22] and experimental [23,24] works with the use of Haan's formula, Eq. (1), which gives the saturation amplitudes of modes. Bearing this fact in mind, we here present a formula for the saturation amplitude of the k_0 mode based on the results obtained and discuss its relations with Haan's formula.

We derive a formula for the saturation amplitude of the k_0 mode in the RP case. By introducing $S(k_0)$, which denotes the amplitude of marginally saturated modes, we can express the rms saturation amplitude as

$$\xi_{rms}=\sqrt{\sum_k \xi_k^2}\approx\sqrt{N_{state}}S(k_0), \tag{20}$$

where N_{state} is the number of states defined by the product of the bandwidth and the density of state $(L/2\pi)$, i.e., $N_{state}=\delta kL/2\pi$ for the 2D case and $N_{state}=\pi(\delta kL/2\pi)^2$ for 3D case. The density of state is the reciprocal of the minimum wave number $\delta k_{min}(=2\pi/L)$ used in Sec. III A. Solving Eq. (20) for $S(k_0)$, we obtain

$$S(k_0)\approx\frac{\xi_{rms}}{\sqrt{N_{state}}}. \tag{21}$$

As shown in Sec. III B, with the fixed Atwood number the saturation amplitude of the rms is almost independent of the initial bandwidth, and is approximately a constant value for the fixed Atwood number in the RP case. If it is independent of the number of states, we expect the saturation amplitude of modes $S(k_0)$ to be inversely proportional to the square root of the number of states. Since the number of states is the product of the bandwidth and the density of state, we show the dependence of the saturation amplitudes of both the rms and the k_0 mode on them. In this subsection, we use the Gaussian distribution function for the initial spectrum and choose $\alpha=0.8$. Figure 7(a) shows the saturation amplitudes as a function of the initial bandwidth with the fixed density of state $k_0L/2\pi=768$, while Fig. 7(b) shows these as a function of the density of state with the fixed bandwidth $\delta k/k_0=1.6\times10^{-2}$. The saturation amplitudes in Fig. 7 are ensemble averaged. Error bars correspond to the rms deviation of the data. Open and closed symbols are the saturation amplitude of the rms and k_0 mode, respectively. Triangles and circles are results for 2D and 3D, respectively. First of all, from Fig. 7, the saturation amplitude of the rms is almost

independent of the number of states, and is approximately a constant value. Thus, the saturation amplitude of the k_0 mode is inversely proportional to the square root of the number of states as expected: $\xi_{rms} \propto \sqrt{N_{state}}^{-1} = (2\sqrt{\pi}/L)/\delta k$ for the 3D case and $\xi_{rms} \propto \sqrt{N_{state}}^{-1} = \sqrt{(2\pi/L)/\delta k}$ for the 2D case, respectively. As shown in the error bars of the saturation amplitude of the rms in Fig. 7, the error decreases as the number of states increases. This decrease of the errors indicates that the fundamental assumption in Haan's saturation formula, i.e., the rms determines the saturation, becomes an appropriate approximation for the large number of states.

Specifying N_{state} in Eq. (21), we obtain

$$S(k_0) \approx \begin{cases} \dfrac{\nu'}{\epsilon' L k_0^2}, & \nu' \equiv 2\sqrt{\pi}\eta' \quad \text{for 3D} \\ \dfrac{\nu'}{\sqrt{\epsilon' L k_0^3}}, & \nu' \equiv \sqrt{2\pi}\eta' \quad \text{for 2D,} \end{cases} \tag{22}$$

where ϵ' ($\equiv \delta k/k_0$) is a normalized spectral width, and η' ($\equiv k_0 \xi_{rms}$) is a normalized saturation amplitude of the rms. As shown in Eq. (22), two independent parameters of η' and ϵ' determine the saturation amplitude $S(k_0)$. Haan has used the same relation as Eq. (22) in his derivation of Eq. (1). From the comparison of Eqs. (1) and (22), we obtain a relation $\nu = \nu'/\epsilon' = 2\sqrt{\pi}\eta'/\epsilon'$ for the 3D case. The saturation amplitude of the rms (η') depends on the Atwood number because that of the LMA depends on it as discussed in a previous section.

In Eq. (22), for $\alpha = 1$ the saturation amplitude $\eta' \approx 0.23$ (see Fig. 5). Then $\nu = \nu'/\epsilon' = 2\sqrt{\pi}\eta'/\epsilon' \approx 2$ if $\epsilon' \approx 0.4$. But, we do not obtain any evidence that ν is a constant as assumed in Refs. [2,8] because the bandwidth ϵ' depends on the initial condition. As implied from the error bars in Fig. 7, the formula has an error of 20–30 %.

IV. CONCLUSION

We have developed a weakly nonlinear theory of the three-dimensional Rayleigh-Taylor instability (RTI) for an arbitrary perturbation with a small but finite bandwidth. By taking third-order nonlinearity into account, we have shown, in detail, the derivation of coupled partial differential equations that describe a continuous transition from the linear to the weakly nonlinear growths of the RTI. Analytical results agree fairly well with two-dimensional hydrodynamic simulations including phase changes of modes due to the mode coupling in the weakly nonlinear regime.

We have investigated the onset of the linear growth saturation for two different spectra of initial perturbations, i.e., the random phase (RP) and no phase difference (NPD) among modes. The theory reveals that the saturation of the linear growth occurs locally. Namely, each of the local maximum amplitudes (LMA's) starts to saturate when it reaches almost the same amplitude that depends on the Atwood number. Therefore, in the case of a large number of states, the root mean square amplitude saturates with almost the same amplitude as the LMA after most of the LMAs reach the saturation amplitude. When the number of states is very large, this result verifies one of Haan's assumptions, i.e., the saturation of the linear growth of the k_0 mode occurs as the rms amplitude reaches a certain value.

The saturation amplitude of the LMA and thus that of the rms are found to be independent of the number of states in the RP case, although the spectral distribution of the perturbation determines the LMA. Since the number of states is given by the product of the bandwidth and the density of states, the saturation amplitude of the k_0 mode could be proportional to the reciprocal of the bandwidth. Although the spectral broadening occurs in the weakly nonlinear regime, the bandwidth at the saturation of the rms still depends on its initial value within our model. In the derivation of Haan's formula, he assumed that the bandwidth, which determined the net perturbation, could be a certain value. This discrepancy between our theory and Haan's formula remains unresolved. In the case that the phases among the modes have some correlations and there exist a few peaks with large amplitudes, the rms amplitude may saturate at a smaller amplitude than the LMAs with the increase of the bandwidth, since the saturation is determined essentially from the LMA.

The theory also shows that after the saturation the LMA grows linearly in time and that its speed is approximated by the product of the linear growth rate and the saturation amplitude. We have studied the dependence of both the saturation amplitude and the weakly nonlinear growth on the Atwood number. With the increase of the Atwood number, the saturation amplitude decreases, while the weakly nonlinear growth increases slightly.

ACKNOWLEDGMENTS

One of the authors (K.N.) would like to express his sincere thanks to Dr. S. W. Haan for valuable discussions on the saturation amplitude of the linear growth. Computations were done on NEC SX-5 at Cybermedia Center, Osaka University.

APPENDIX A: DERIVATION OF COUPLED PARTIAL DIFFERENTIAL EQUATIONS

We show the details of derivation of the coupled partial differential equations. Since we consider up to the third-order nonlinearity of the fundamental mode, for $2k_0$ and $0k_0$ modes we take into account up to the second-order nonlinearity. Thus in nonlinear terms for $2\boldsymbol{k}_0$ and $0\boldsymbol{k}_0$, we can treat $\phi_L^{(1)} = -\phi_H^{(1)}$, $\xi^{(1)} = \partial\phi_H^{(1)}/\partial t$ from Eqs. (13a), (14a), and (14b). Then subtracting Eq. (14d) from Eq. (14c), we obtain

$$\phi_L^{(2)} = -\phi_H^{(2)} + \sqrt{2}\phi_H^{(1)} \frac{\partial \phi_H^{(1)}}{\partial t}. \tag{A1}$$

By substituting Eq. (A1) into Eq. (13b), we have

$$\xi^{(2)}=\frac{\partial\phi_H^{(2)}}{\partial t}-\frac{\sqrt{2}}{2}\left(\frac{\partial\phi_H^{(1)}}{\partial t}\right)^2-\frac{\sqrt{2}(1-\alpha)}{2}\phi_H^{(1)2}. \quad \text{(A2)}$$

After taking the time derivative of Eq. (A2) and eliminating $\partial\xi^{(2)}/\partial t$ by using Eq. (14c), we obtain Eq. (15b). In the same way, we obtain

$$\xi^{(0)}=\frac{\partial\phi_H^{(0)}}{\partial t}-\alpha|\phi_H^{(1)}|^2-\alpha\left|\frac{\partial\phi_H^{(1)}}{\partial t}\right|^2 \quad \text{(A3)}$$

from Eq. (13c). By taking the time derivative of Eq. (A3), we have

$$\frac{\partial^2\phi_H^{(0)}}{\partial t^2}=2\alpha\left(\frac{\partial\phi_H^{(1)*}}{\partial t}\phi_H^{(1)}+\phi_H^{(1)*}\frac{\partial\phi_H^{(1)}}{\partial t}\right), \quad \text{(A4)}$$

where we have used $\partial\xi^{(0)}/\partial t=0$. By elimination of $\partial\xi^{(1)}/\partial t$ from Eqs. (14a) and (14b), and using Eqs. (A1) and (A2) we obtain

$$\begin{aligned}\phi_L^{(1)}=&-\phi_H^{(1)}+2\frac{\partial\phi_H^{(0)}}{\partial t}\phi_H^{(1)}+2\sqrt{2}\,\frac{\partial\phi_H^{(1)*}}{\partial t}\phi_H^{(2)}\\&-\sqrt{2}\phi_H^{(1)*}\frac{\partial\phi_H^{(2)}}{\partial t}-2(\alpha+1)\left|\frac{\partial\phi_H^{(1)}}{\partial t}\right|^2\phi_H^{(1)}\\&+\phi_H^{(1)*}\left(\frac{\partial\phi_H^{(1)}}{\partial t}\right)^2-(3\alpha-1)|\phi_H^{(1)}|^2\phi_H^{(1)}. \quad \text{(A5)}\end{aligned}$$

By substituting Eqs. (A2) and (A3) into Eq. (14a), we obtain

$$\begin{aligned}\frac{\partial\xi^{(1)}}{\partial t}=&\phi_H^{(1)}-i(\hat{\boldsymbol{k}}_0\cdot\boldsymbol{\nabla})\phi_H^{(1)}-\frac{1}{2}|\hat{\boldsymbol{k}}_0\times\boldsymbol{\nabla}|^2\phi_H^{(1)}-\frac{\partial\phi_H^{(0)}}{\partial t}\phi_H^{(1)}\\&-\sqrt{2}\,\frac{\partial\phi_H^{(1)*}}{\partial t}\phi_H^{(2)}+\frac{\sqrt{2}}{2}\phi_H^{(1)*}\frac{\partial\phi_H^{(2)}}{\partial t}\\&+\frac{2\alpha+1}{2}\left|\frac{\partial\phi_H^{(1)}}{\partial t}\right|^2\phi_H^{(1)}-\frac{3}{4}\phi_H^{(1)*}\left(\frac{\partial\phi_H^{(1)}}{\partial t}\right)^2\\&+\frac{3\alpha-1}{2}|\phi_H^{(1)}|^2\phi_H^{(1)}. \quad \text{(A6)}\end{aligned}$$

By using Eqs. (13c), (A1), and (A2), and the time derivative of Eq. (A5), we obtain from (13a),

$$\begin{aligned}\xi^{(1)}=&\frac{\partial\phi_H^{(1)}}{\partial t}-\frac{\partial\phi_H^{(0)}}{\partial t}\frac{\partial\phi_H^{(1)}}{\partial t}-\frac{1+2\alpha}{\sqrt{2}}\frac{\partial\phi_H^{(1)*}}{\partial t}\frac{\partial\phi_H^{(2)}}{\partial t}\\&+\frac{(\gamma_2^2-2)-(\gamma_2^2+2)\alpha}{\sqrt{2}}\phi_H^{(1)*}\phi_H^{(2)}\\&+\frac{8\alpha+1}{4}\left|\frac{\partial\phi_H^{(1)}}{\partial t}\right|^2\frac{\partial\phi_H^{(1)}}{\partial t}\\&+\frac{(2\alpha-1)(1-\alpha)}{2}\frac{\partial\phi_H^{(1)*}}{\partial t}\phi_H^{(1)2}+3\alpha|\phi_H^{(1)}|^2\frac{\partial\phi_H^{(1)}}{\partial t}. \quad \text{(A7)}\end{aligned}$$

By elimination of $\partial\xi^{(1)}/\partial t$ from Eq. (A6) and the time derivative of Eq. (A7), we obtain Eq. (15a).

APPENDIX B: PARTIAL DIFFERENTIAL EQUATION FOR THIRD HARMONIC

Let us derive the partial differential equation for the third harmonic corresponding to Eq. (15a). This procedure is done in the same manner as the fundamental. Substituting the expansion for ξ, ϕ_H, and ϕ_L into the expanded equations (4) and (5) and picking up the terms associated with $e^{i3\boldsymbol{k}_0\cdot\boldsymbol{x}}$ yields the following system of coupled equations:

$$\frac{\partial\xi^{(3)}}{\partial t}=3\phi_H^{(3)}-\frac{3\sqrt{2}}{2}\phi_H^{(1)}\xi^{(2)}-3\sqrt{2}\xi^{(1)}\phi_H^{(2)}+\frac{3}{4}\xi^{(1)2}\phi_H^{(1)}. \quad \text{(B1)}$$

$$\begin{aligned}=&-3\phi_L^{(3)}-\frac{3\sqrt{2}}{2}\phi_L^{(1)}\xi^{(2)}-3\sqrt{2}\xi^{(1)}\phi_L^{(2)}\\&-\frac{3}{4}\xi^{(1)2}\phi_L^{(1)}. \quad \text{(B2)}\end{aligned}$$

$$\begin{aligned}\frac{1+\alpha}{2}&\left(\frac{\partial\phi_H^{(3)}}{\partial t}-\sqrt{2}\xi^{(1)}\frac{\partial\phi_H^{(2)}}{\partial t}-\frac{\sqrt{2}}{2}\frac{\partial\phi_H^{(1)}}{\partial t}\xi^{(2)}+\frac{1}{4}\xi^{(1)2}\frac{\partial\phi_H^{(1)}}{\partial t}\right.\\&\left.-\frac{\xi^{(3)}}{\alpha}\right)=\frac{1-\alpha}{2}\left(\frac{\partial\phi_L^{(3)}}{\partial t}+\sqrt{2}\xi^{(1)}\frac{\partial\phi_L^{(2)}}{\partial t}+\frac{\sqrt{2}}{2}\frac{\partial\phi_L^{(1)}}{\partial t}\xi^{(2)}\right.\\&\left.+\frac{1}{4}\xi^{(1)2}\frac{\partial\phi_L^{(1)}}{\partial t}-\frac{\xi^{(3)}}{\alpha}\right). \quad \text{(B3)}\end{aligned}$$

Subtracting Eqs. (B1) and (B2),

$$\begin{aligned}\phi_L^{(3)}=&-\phi_H^{(3)}+\sqrt{2}\phi_H^{(1)}\frac{\partial\phi_H^{(2)}}{\partial t}+2\sqrt{2}\,\frac{\partial\phi_H^{(1)}}{\partial t}\phi_H^{(2)}\\&+(\alpha-1)\phi_H^{(1)3}-3\phi_H^{(1)}\left(\frac{\partial\phi_H^{(1)}}{\partial t}\right)^2. \quad \text{(B4)}\end{aligned}$$

Substituting the time derivative of this into Eq. (B3), we obtain

$$\xi^{(3)}=\frac{\partial\phi_H^{(3)}}{\partial t}-\frac{3\sqrt{2}}{2}\frac{\partial\phi_H^{(1)}}{\partial t}\frac{\partial\phi_H^{(2)}}{\partial t}+\frac{\sqrt{2}(\alpha-1)}{2}(2+\gamma_2^2)\phi_H^{(1)}\phi_H^{(2)}+\frac{3}{4}\left(\frac{\partial\phi_H^{(1)}}{\partial t}\right)^3+\frac{5(1-\alpha)}{2}\phi_H^{(1)2}\frac{\partial\phi_H^{(1)}}{\partial t}. \tag{B5}$$

Elimination of $\partial\xi^{(3)}/\partial t$ from Eq. (B1) and the time derivative of Eq. (B5) leads to

$$\frac{\partial^2\phi_H^{(3)}}{\partial t^2}=3\phi_H^{(3)}+\frac{\sqrt{2}}{2}(\gamma_2^2+2)(1-\alpha)\phi_H^{(1)}\frac{\partial\phi_H^{(2)}}{\partial t}-\frac{\sqrt{2}}{2}[(\gamma_2^2+2)\alpha+4(1-\gamma_2^2)]\frac{\partial\phi_H^{(1)}}{\partial t}\phi_H^{(2)}+(\alpha-1)\phi_H^{(1)3}+2(\alpha-1)\phi_H^{(1)}\left(\frac{\partial\phi_H^{(1)}}{\partial t}\right)^2. \tag{B6}$$

This is the partial differential equation for the third harmonic. The amplitude of the third harmonic can be evaluated from Eq. (B5) using $\phi_H^{(3)}$ obtained from Eq. (B6).

[1] G.I. Taylor, Proc. R. Soc. London, Ser. A **201**, 192 (1950).
[2] S.W. Haan, Phys. Rev. A **39**, 5812 (1989).
[3] D.H. Sharp, Physica D **12**, 3 (1984).
[4] D.L. Youngs, Physica D **12**, 32 (1984).
[5] M.J. Dunning and S.W. Haan, Phys. Plasmas **2**, 1669 (1995).
[6] D. Shvarts, U. Alon, D. Ofer, R.L. McCrory, and C.P. Verdon, Phys. Plasmas **2**, 2465 (1995).
[7] D. Ofer, U. Alon, D. Shvarts, R.L. McCrory, and C.P. Verdon, Phys. Plasmas **3**, 3073 (1996).
[8] S.W. Haan, Phys. Fluids B **3**, 2349 (1991).
[9] J.W. Jacobs and I. Catton, J. Fluid Mech. **187**, 329 (1988).
[10] K. Nishihara and T. Ikegawa, J. Plasma Fusion Res. **2**, 536 (1999).
[11] T. Ikegawa and K. Nishihara, in *Inertial Fusion Sciences and Applications 99*, edited by C. Labaune *et al.* (Elsevier, New York, 2000), p. 228.
[12] T. Ikegawa and K. Nishihara, Phys. Rev. Lett. **89**, 115001 (2002).
[13] H. Takabe and A. Yamamoto, Phys. Rev. A **44**, 5142 (1991).
[14] U. Alon, J. Hecht, D. Ofer, and D. Shvarts, Phys. Rev. Lett. **74**, 534 (1995).
[15] V.N. Goncharov, Phys. Rev. Lett. **88**, 134502 (2002).
[16] D. Layzer, Astrophys. J. **122**, 1 (1955).
[17] A.H. Nayfeh, J. Fluid Mech. **38**, 619 (1969).
[18] J.W. Miles, J. Fluid Mech. **75**, 419 (1976).
[19] H. Sakagami and K. Nishihara, Phys. Fluids B **2**, 2715 (1990).
[20] M.M. Marinak, S.G. Glendinning, R.J. Wallace, B.A. Remington, K.S. Budil, S.W. Haan, R.E. Tipton, and J.D. Kilkenny, Phys. Rev. Lett. **80**, 4426 (1998).
[21] J.P. Dahlburg, D.E. Fyfe, J.H. Gardner, S.W. Haan, S.E. Bodner, and G.D. Doden, Phys. Plasmas **2**, 2453 (1995).
[22] R.J. Taylor, J.P. Dahlburg, A. Iwase, J.H. Gardner, D.E. Fyfe, and O. Willi, Phys. Rev. Lett. **76**, 1643 (1996).
[23] B.A. Remington, S.V. Weber, M.M. Marinak, S.W. Haan, J.D. Kilkenny, R.J. Wannce, and G. Kimonte, Phys. Plasmas **2**, 241 (1995).
[24] V.A. Smalyuk *et al.*, Phys. Rev. Lett. **81**, 5342 (1998); Phys. Plasmas **6**, 4022 (1999).